

Structure of Pion Photoproduction Amplitudes

V. Mathieu,^{1,2,*} J. Nys,³ A. H. Blin,⁴ C. Fernández-Ramírez,⁵ A. Jackura,^{1,2}
M. Mikhasenko,⁶ V. Pauk,⁷ A. Pilloni,⁷ A. P. Szczepaniak,^{1,2,7} and G. Fox⁸

(Joint Physics Analysis Center)

¹*Center for Exploration of Energy and Matter, Indiana University, Bloomington, IN 47403*

²*Physics Department, Indiana University, Bloomington, IN 47405, USA*

³*Department of Physics and Astronomy, Ghent University, Belgium*

⁴*Departamento de Física Teórica and IFIC, Centro Mixto Universidad de Valencia-CSIC, Institutos de Investigación de Paterna, E-46071 Valencia, Spain*

⁵*Instituto de Ciencias Nucleares, Universidad Nacional Autónoma de México, Ciudad de México 04510, Mexico*

⁶*Universität Bonn, Helmholtz-Institut für Strahlen- und Kernphysik, 53115 Bonn, Germany*

⁷*Theory Center, Thomas Jefferson National Accelerator Facility 12000 Jefferson Avenue, Newport News, VA 23606, USA*

⁸*School of Informatics and Computing, Indiana University, Bloomington, IN 47405, USA*

We derived and apply the finite energy sum rules in pion photoproduction. We reconstruct the left-hand-side of the sum rules using several low-energy models. It is shown how the low energy models and the sum rules can be used to make quantitative predictions for the high-energy observables. A model, in terms of a Regge-pole expansion, that matches the sum rules and the high-energy observables is presented.

I. INTRODUCTION

The photoproduction of a single pion was the first measurements performed with the GlueX detector [1] and will be one of the first measurements performed with the CLAS12 detector [2] at the Jefferson Lab facility (JLab). At low energies, this reaction forms an invaluable source of information about the baryon excitation spectrum [3–8]. At high energies it reveals details of the residual hadron interactions due to cross-channel particle (Reggeon) exchanges [9]. These two energy regimes are analytically connected, a feature that can be used to relate properties of resonances in the direct channel to Reggeons in the crossed channels. In practice this can be accomplished through dispersion relations and finite-energy sum rules (FESR) [10, 11].

There are several models in the literature focusing on the neutral and charged pion photoproductions in the high energy region [12–20]. The diversity between these models essential originates from the unconstrained residues. Several authors used the FESR to constraint the residues in neutral [21–23] and charged [24–26] pion photoproduction independently. To our knowledge only Worden performed a global fit of both neutral and pion photoproduction constrained with the FESR [27]. However the low energy models used for the left-hand-side (LHS) of the sum rules were not constraint by the high energy data. At best, fixed t dispersion relations were imposed to determine the baryon spectrum in Ref. [28–31] but, to our knowledge, FESR in photoproduction are not fully exploited for constraining the low-energy models.

Although a comparative study of FESR in hadro- and photo-production [32] shed light into the difficulties as-

sociated with FESR in pion photoproduction, we believe that these constraints are the ideal tools to improve the knowledge of the excited baryon spectrum. Indeed, according to the Review of Particle Properties [33], the N^* and Δ spectra below 2 GeV are “at least fairly well explored”, while the properties of their resonances above 2 GeV are poorly known. The 2-3 GeV energy range is the transition between the baryon resonance region and the Regge regime. Since the number of relevant partial waves increases with energy, additional tools are required to constrain the amplitude construction. FESR, which relate these energy regions, is therefore the ideal tool to better constrain the baryon resonances above 2 GeV.

With the forthcoming CLAS12 detector who will cover both the resonance and the high energy regions, there is a growing interest in the excited baryon spectrum and its transition to Regge region. The purpose of this paper is then to bring up to date the FESR framework, point out the mismatch between both sides of the sum rules and propose a parametrization of the high energy region that could be a starting point for a combined fit of both the low and high energy regions. This study complements our similar FESR analysis of η photoproduction [34] and pion-nucleon scattering [35].

Our starting point, in Sec. II, is to decompose the amplitudes into form factors (or scalar amplitudes) which multiply a covariant amplitude base. The singularities of these scalar amplitudes are only the ones required by unitarity and are therefore suitable for a dispersive analysis. After reviewing the properties of the scalar amplitudes, we will use dispersion relations and a standard Regge parametrization to derive their FESR in Sec. III. We then evaluate the low-energy side of the sum rules with various available models in Sec. IV and extract, from this side for the sum, the effective Regge residues in Sec. V. We then show in Sec. VI that, assuming the dominance of a single Regge pole, the low-energy models provide qual-

* corresponding author: mathieuv@indiana.edu

itative predictions for the observables at high energies. We continue our analysis in Sec. VII by presenting a combined fit of the parameters in the Regge expansion to both the FESR and the high-energy observables. Finally our conclusions are presented in Sec. VIII.

II. FORMALISM: SCALAR AMPLITUDES

The photoproduction of a pion off a nucleon (proton or neutron) target:

$$\gamma(k, \lambda_\gamma) + N(p, \lambda) \longrightarrow \pi(q) + N'(p', \lambda') \quad (1)$$

depends on three helicities and the two Mandelstam variables: the center-of-mass energy squared $s = (k+p)^2$ and the momentum transferred squared $t = (q-k)^2$. The third Mandelstam variable $u = (p'-k)^2$ is linked by the relation $s + t + u = 2M_N^2 + \mu^2 \equiv \Sigma$ where M_N is the nucleon mass and μ the pion mass. All other masses will be denoted by m_x for a meson x .

In the reaction (1), we used the s -channel center-of-mass helicities λ_γ, λ and λ' . The s -channel frame is, by convention, the process (1) in its center-of-mass frame. The t -channel frame refers to the crossed-channel reaction $\gamma\pi \rightarrow \bar{N}N'$ in its center-of-mass frame.

The photoproduction of a pseudoscalar is fully described by four scalar amplitudes. The standard decomposition [36] of the s -channel helicity amplitudes reads

$$A_{\lambda'; \lambda \lambda_\gamma}(s, t) = \bar{u}_{\lambda'}(p') \left(\sum_{k=1}^4 A_k(s, t) M_k \right) u_\lambda(p). \quad (2)$$

The definition of the covariant basis $M_k \equiv M_k(s, t, \lambda_\gamma)$ and all relevant kinematical quantities is given in the Appendices of Ref. [20].

In this work, we will assume that isospin is a good symmetry. Writing explicitly the isospin indices (i, j for the target and recoil nucleon respectively and a for the isovector pion), the standard isospin decomposition for the scalar amplitudes reads

$$A_{ji}^a = A^{(+)} \delta^{a3} \delta_{ji} + A^{(-)} \frac{1}{2} [\tau^a, \tau^3]_{ji} + A^{(0)} \tau_{ji}^a \quad (3)$$

with τ the Pauli isospin matrices. In this basis, the isospin indices correspond to good isospin I and G -parity of $\gamma\pi$. More explicitly, the t -channel (*i.e.* exchange) quantum numbers of the scalar amplitudes are

$$I^G(A^{(0)}) = 1^+ \quad I^G(A^{(+)}) = 0^- \quad I^G(A^{(-)}) = 1^-. \quad (4)$$

The charged and neutral pion photoproduction reactions are described by an appropriate combination of the isospin components of the scalar amplitudes. Schematically, the contributions of isospin amplitudes to the he-

licity amplitudes are

$$\gamma p \rightarrow \pi^+ n : \sqrt{2} \left(A^{(0)} + A^{(-)} \right) \quad (5a)$$

$$\gamma n \rightarrow \pi^- p : \sqrt{2} \left(A^{(0)} - A^{(-)} \right) \quad (5b)$$

$$\gamma p \rightarrow \pi^0 p : A^{(+)} + A^{(0)} \quad (5c)$$

$$\gamma n \rightarrow \pi^0 n : A^{(+)} - A^{(0)}. \quad (5d)$$

The u -channel, $\gamma\bar{N} \rightarrow \pi\bar{N}$, is obtained from the s -channel by charge conjugation. Conservation of charge conjugation implies then a symmetry of the scalar amplitudes under the transformation $s \leftrightarrow u$. This symmetry can be exploited by using the crossing variable

$$\nu = \frac{s-u}{4M_N} = E_{\text{lab}} + \frac{t-\mu^2}{4M_N}, \quad (6)$$

with E_{lab} the photon energy in the laboratory frame (target rest frame). The scalar amplitudes can be categorized into crossing-even

$$\begin{aligned} A_{1,2,4}^{(0,+)}(-\nu - i\epsilon, t) &= +A_{1,2,4}^{(0,+)}(\nu + i\epsilon, t) \\ A_3^{(-)}(-\nu - i\epsilon, t) &= +A_3^{(-)}(\nu + i\epsilon, t) \end{aligned} \quad (7a)$$

and crossing-odd

$$\begin{aligned} A_{1,2,4}^{(-)}(-\nu - i\epsilon, t) &= -A_{1,2,4}^{(-)}(\nu + i\epsilon, t), \\ A_3^{(0,+)}(-\nu - i\epsilon, t) &= -A_3^{(0,+)}(\nu + i\epsilon, t) \end{aligned} \quad (7b)$$

functions. In Eq. (7), ϵ is a small and positive quantity indicating on which side of the unitarity cut the function is evaluated.

In the Appendix of Ref. [20] (and references therein), we proved that the scalar amplitudes A_1, A_3, A_4 as well as the combination $A_1 + tA_2$ have good t -channel parity P and G -parity. For convenience we define

$$A'_2 \equiv A_1 + tA_2. \quad (8)$$

Table I summarizes the t -channel quantum numbers of the scalar amplitudes. In view of the symmetry relations (7) and Table I, we note that, with these standard conventions, the crossing-even (crossing-odd) amplitudes involve negative (positive) signature $\tau = (-1)^J$ exchanges. The exchanges are also divided into two other categories: the natural exchanges ($P(-1)^J = +1$) and the unnatural exchanges ($P(-1)^J = -1$). In addition to the signature and naturality of the exchanges we added in Table I the lowest spins and the name of the leading trajectory. We did not indicate the quantum numbers 0^{++} in the a_2 trajectory since the $a_0(980)$ meson lies on the daughter trajectory.

Since crossed-channel exchanges control the behavior of the helicity amplitudes at high-energy [9, 37], the t -channel quantum numbers of the scalar amplitudes are essential to determine their relative importance in the high energy region. Empirically, Regge trajectories

TABLE I. Invariant amplitudes A_i with corresponding t -channel exchanges. I is isospin, G is G -parity, J is total spin, P is parity, C is charge conjugation and $\tau = (-1)^J$ is the signature. The spin of the lightest meson on the trajectory is indicated in the last column.

$A_i^{(\sigma)}$	I^G	$P(-1)^J$	τ	J^{PC}	Lightest meson
$A_{1,4}^{(0)}$	1^+	$+1$	-1	$(1, 3, 5, \dots)^{--}$	$\rho(770)$
$A_{1,4}^{(+)}$	0^-	$+1$	-1	$(1, 3, 5, \dots)^{--}$	$\omega(782)$
$A_{1,4}^{(-)}$	1^-	$+1$	$+1$	$(2, 4, 6, \dots)^{++}$	$a_2(1320)$
$A_2^{(0)}$	1^+	-1	-1	$(1, 3, 5, \dots)^{+-}$	$b_1(1235)$
$A_2^{(+)}$	0^-	-1	-1	$(1, 3, 5, \dots)^{+-}$	$h_1(1170)$
$A_2^{(-)}$	1^-	-1	$+1$	$(0, 2, 6, \dots)^{-+}$	$\pi(140)$
$A_3^{(0)}$	1^+	-1	$+1$	$(2, 4, 6, \dots)^{--}$	$\rho_2(-)$
$A_3^{(+)}$	0^-	-1	$+1$	$(2, 4, 6, \dots)^{--}$	$\omega_2(-)$
$A_3^{(-)}$	1^-	-1	-1	$(1, 2, 5, \dots)^{++}$	$a_1(1260)$

involving natural exchanges dominate over unnatural trajectories. Table I indicates that the scalar amplitudes A_1 and A_4 should contain the main contribution to the observables at high energies. We can obtain further indications of the high-energy behavior of the scalar amplitudes from their relation to the helicity amplitudes in the leading s approximation: (the notation $\pm = \pm\frac{1}{2}$ is used for the nucleon helicities)

$$\sqrt{-t}A_4 = \frac{1}{\sqrt{2s}} (A_{+;+1} + A_{-;-1}) \quad (9a)$$

$$\sqrt{-t}A_3 = \frac{1}{\sqrt{2s}} (A_{+;+1} - A_{-;-1}) \quad (9b)$$

$$A_1 = \frac{1}{\sqrt{2s}} (A_{+;-1} - A_{-;+1}) \quad (9c)$$

$$A_2' = \frac{-1}{\sqrt{2s}} (A_{+;-1} + A_{-;+1}). \quad (9d)$$

These relations show that, at the leading order in the energy squared, A_4 and A_3 are helicity non-flip at the nucleon vertex and, A_1 and A_2' are helicity flip at the nucleon vertex. It is well-known that isoscalar (isovector) exchanges are predominantly helicity non-flip (helicity flip) at the nucleon vertex [9]. We then expect $A_4^{(+)}$ and $A_1^{(0,-)}$ to be the largest amplitudes at high energy.

Finally, the factorization of Regge pole residues yields a simple form for the kinematical singularities in t at high energy [38]

$$A_{\lambda\gamma;\lambda\lambda\gamma}(\nu, t) \propto (\sqrt{-t})^{|\lambda_\gamma|+|\lambda'-\lambda|} \quad (10)$$

From Eqs. (9) and (10), the Regge pole contributions in A_1 and A_2' vanish in the forward direction, *i.e.* $A_1 \propto t$

and $A_2' \propto t$. Having described the properties of the scalar form factors, we now turn our attention to their analytic structure and derive the FESR in the next section.

III. FINITE ENERGY SUM RULES

The starting point of the derivation is the analytic structure of the scalar amplitudes. The analytic structure and the associated dispersion relation for pion photoproduction were discussed extensively in the literature [36, 39–41]. Every scalar function has a nucleon pole and a left- and right-hand cuts required by unitarity, which are represented in the complex ν plane in Fig. 1. The nucleon pole term is written, in our convention, as

$$A_i^{(\sigma)} \Big|_{\text{pole}} = B_i^{(\sigma)} \left(\frac{1}{\nu - \nu_B} + \frac{\tau_i^{(\sigma)}}{\nu + \nu_B} \right), \quad (11)$$

with $\nu_B = (t - \mu^2)/(4M_N)$ the crossing variable at the nucleon pole and $B_i^{(\sigma)} \equiv B_i^{(\sigma)}(t)$. The nucleon pole residues $B_i^{(\sigma)}$ are tabulated in Table II. According to Table I, the crossing-even (crossing-odd) scalar amplitudes correspond to Reggeons with negative (positive) signature $\tau_i^{(\sigma)} = -1$ ($\tau_i^{(\sigma)} = +1$).

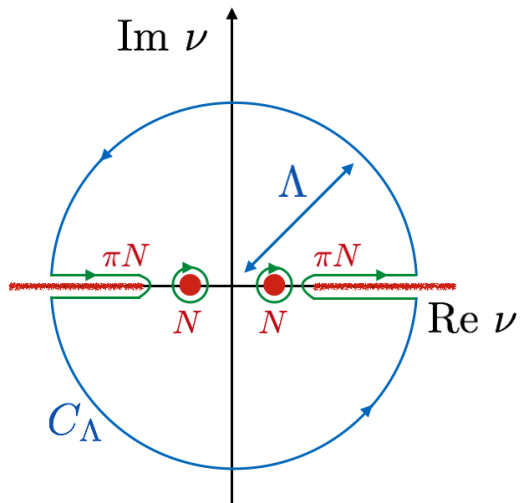


FIG. 1. The complex ν plane. The singularities (nucleon pole and the two cuts starting at the πN threshold) are in red. The integration contour is divided into two pieces as in Eq. (12), the contour surrounding the discontinuities and the circle C_Λ of radius Λ .

Let us now consider the function $\nu^k A_i(\nu, t)$ (omitting the isospin index) with k being a positive integer. The function $\nu^k A_i(\nu, t)$ has the same analytic structure as $A_i(\nu, t)$. Deriving the sum rules for $\nu^k A_i(\nu, t)$ instead of $A_i(\nu, t)$ will provide us a set of constraints, or moments. According to the Cauchy theorem the contour integral in Fig. 1 vanishes. Equivalently, we can match the discontinuity on the real axis to the integral along the circle of

TABLE II. Born term in the DR

(σ)	(0)	(+)	(-)	
$B_1^{(\sigma)}$	$-\frac{eg}{2M_N} \frac{1}{2}$	$-\frac{eg}{2M_N} \frac{1}{2}$	$-\frac{eg}{2M_N} \frac{1}{2}$	$e = 0.303$
$B_2^{(\sigma)}$	$\frac{eg}{2M_N} \frac{1}{t-\mu^2}$	$\frac{eg}{2M_N} \frac{1}{t-\mu^2}$	$\frac{eg}{2M_N} \frac{1}{t-\mu^2}$	$g = 13.54$
$B_3^{(\sigma)}$	$\frac{eg}{2M_N} \frac{\kappa_p + \kappa_n}{4M_N}$	$\frac{eg}{2M_N} \frac{\kappa_p - \kappa_n}{4M_N}$	$\frac{eg}{2M_N} \frac{\kappa_p - \kappa_n}{4M_N}$	$\kappa_p = 1.78$
$B_4^{(\sigma)}$	$\frac{eg}{2M_N} \frac{\kappa_p + \kappa_n}{4M_N}$	$\frac{eg}{2M_N} \frac{\kappa_p - \kappa_n}{4M_N}$	$\frac{eg}{2M_N} \frac{\kappa_p - \kappa_n}{4M_N}$	$\kappa_n = -1.91$

radius Λ (by convention we include the nucleon poles in the discontinuities as in Fig. 1)

$$\int_0^\Lambda [D_{i,R}(\nu, t) + (-1)^k D_{i,L}(\nu, t)] \nu^k \frac{d\nu}{2i} = - \int_{C_\Lambda} A_i(\nu, t) \nu^k \frac{d\nu}{2i}. \quad (12)$$

For $\nu > 0$ $D_{i,R}$ and $D_{i,L}$ correspond to the discontinuities along the s -channel (right) and u -channel (left) unitarity cuts respectively:

$$D_{i,R}(\nu, t) = \lim_{\epsilon \rightarrow 0} [A_i(+\nu + i\epsilon, t) - A_i(+\nu - i\epsilon, t)] \quad (13a)$$

$$D_{i,L}(\nu, t) = \lim_{\epsilon \rightarrow 0} [A_i(-\nu + i\epsilon, t) - A_i(-\nu - i\epsilon, t)] \quad (13b)$$

Thanks to the crossing properties of the scalar function, we can relate the left and right discontinuities $D_{i,L}(\nu, t) = \tau_i D_{i,R}(\nu, t)$. The right-hand-side (RHS) of the sum rules (12) becomes

$$[1 + \tau_i(-1)^k] \int_0^\Lambda D_{i,R}(\nu, t) \nu^k \frac{d\nu}{2i}.$$

We then observe that the LHS of Eq. (12) is non zero only for $\tau_i = (-1)^k$ since k is an integer. In other words, crossing-even (crossing-odd) amplitudes require odd (even) moments.

In our convention, the discontinuities include the nucleon pole at ν_B and the unitarity cuts starting at ν_0 , the πN threshold:

$$\nu_0 = \mu + \frac{t + \mu^2}{4M_N}. \quad (14)$$

If $\nu_0 > 0$, the left and right cuts do not overlap and the amplitude is real on a part of the real axis. In this case the discontinuities along the cuts are given by the imaginary part. The contribution of the right hand discontinuity to the sum rules reads

$$\int_0^\Lambda D_{i,R}(\nu, t) \nu^k \frac{d\nu}{2i} = \pi B_i \nu_M^k + \int_{\nu_0}^\Lambda \text{Im} A_i(\nu, t) \nu^k d\nu. \quad (15)$$

If $\nu_0 < 0$, the left and right cuts do overlap, one can nevertheless use a contour passing between the cuts and

obtain the same dispersion relation (12). The discontinuity is still given by the imaginary part along the cut since the function is analytic in t and is real for $t > 0$ along this cut.

To work out the LHS of Eq. (12), we assume that Λ is large enough to approximate the amplitudes by a Regge form along the circle:

$$A_i(\nu, t) = -\beta_i(t) \frac{\tau_i (r_i \nu)^{\alpha_i(t)-1} + (-r_i \nu)^{\alpha_i(t)-1}}{\sin \pi \alpha_i(t)}. \quad (16)$$

τ_i , as for the RHS of Eq. (12), is the signature of the exchange and $r_i > 0$ is a scale factor. $\beta_i(t)$ and $\alpha_i(t)$ are the residue and the trajectory of the Regge pole. The r_i are scale factors required by dimensional analysis. The exponent is such that the helicity amplitudes, cf. Eq. (9), behave as $s^{\alpha(t)}$ at large energies, cf. Eq (9).

Assuming this form, the integral along the circle of radius Λ can be calculated analytically. The integration is performed separately for the two terms in Eq. (16) as they have different cuts, a left-hand cut for the first term and a right-hand cut for the second. The contribution of the contour integral in Eq. (12) of the first term, with the change of variable $\nu = \Lambda e^{i\phi}$, reads

$$\begin{aligned} \tau_i \beta_i(t) \frac{(r_i \Lambda)^{\alpha_i(t)-1}}{2i \sin \pi \alpha_i(t)} \Lambda^{k+1} \int_{-\pi}^{\pi} e^{i\phi(\alpha_i(t)+k)} i d\phi \\ = \tau_i (-1)^k \beta_i(t) \frac{(r_i \Lambda)^{\alpha_i(t)+k}}{\alpha_i(t) + k} \Lambda^{k+1} \end{aligned} \quad (17)$$

if $\alpha_i(t) + k \neq 0$. Since the Regge trajectories satisfy empirically $\alpha(t) > -1$ for $|t| < 4 \text{ GeV}^2$ [42, 43], the moments $k \geq 1$ always satisfy this constraint. The other term yields the contribution to the contour integral:

$$\begin{aligned} -\beta_i(t) \frac{(-r_i \Lambda)^{\alpha_i(t)-1}}{2i \sin \pi \alpha_i(t)} \Lambda^{k+1} \int_0^{2\pi} e^{i\phi(\alpha_i(t)+k)} i d\phi \\ = \beta_i(t) \frac{(r_i \Lambda)^{\alpha_i(t)-1}}{\alpha_i(t) + k} \Lambda^{k+1} \end{aligned} \quad (18)$$

if $\alpha_i(t) + k \neq 0$. As expected the LHS of Eq. (12) also vanishes unless $\tau_i = (-1)^k$. We can then equal the two sides of the sum rules and obtain the finite energy sum rules:

$$\pi B_i \frac{\nu_M^k}{\Lambda^{k+1}} + \int_{\nu_0}^\Lambda \text{Im} A_i(\nu, t) \frac{\nu^k d\nu}{\Lambda^{k+1}} = \beta_i(t) \frac{(r_i \Lambda)^{\alpha_i(t)-1}}{\alpha_i(t) + k}. \quad (19)$$

It should be kept in mind that the FESR (19) are valid only for odd (even) values of k for crossing-even (crossing-odd) amplitudes. In our derivation, we explicitly assumed a single Regge pole for each definite isospin scalar amplitude. In general, the RHS of the FESR will involve as many terms as there are Reggeons contributing to the amplitude.

The sum rule (19) was derived using the known analytic structure of the scalar amplitudes at fixed $t < 0$.

For large negative values of t singularities coming from two fixed poles appear (box diagrams with internal pions and nucleons). They manifest as an additional cut parallel to the unitarity cut. They are nevertheless far from the forward angles region. The closest singularity of the double spectral representation was shown to be at $t = -1.1 \text{ GeV}^2$ and $W > 1.6 \text{ GeV}$ in Ref. [44]. In this work, we will focus on the forward region $-1 > t/\text{GeV}^2 > 0$ and we will not have to include such an additional singularity in the dispersion relations.

IV. THE LOW ENERGY SIDE OF THE SUM RULES

Baryon spectroscopy has been an active field of investigations recently. There are five independent groups determining the baryon spectrum from photoproduction data: MAID [3], SAID [4], Bonn-Gatchina (BnGa) [5], Jülich-Bonn (JüBo) [6] and ANL-Osaka (ANL-O) [7]. We refer to Ref. [8] for a comparison of the different models developed by these groups. In this section we will evaluate the RHS of the sum rules (19) using the latest partial waves analysis by the different groups.

The SAID and MAID groups have included pion photoproduction on a neutron target in their analysis. Their models for the scalar function $A_i^{(\sigma)}$ are available for all isospin configurations $\sigma = 0, +, -$. The latest JüBo and BnGa models were developed for proton targets only. Consequently we can only perform our analysis for the neutral pion photoproduction $\gamma p \rightarrow \pi^0 p$ since the LHC discontinuity of $\gamma p \rightarrow \pi^+ n$ requires the knowledge of $\gamma n \rightarrow \pi^- p$ in the physical region by conjugation invariance.

For our purposes, we quote the domain of validity of the different models and the number of multipoles available in the models

$$\text{MAID: } E_{\text{lab}} \leq 1.66 \text{ GeV and } L \leq 5 \quad (20a)$$

$$\text{SAID: } E_{\text{lab}} \leq 2.40 \text{ GeV and } L \leq 5 \quad (20b)$$

$$\text{JüBo: } E_{\text{lab}} \leq 2.57 \text{ GeV and } L \leq 5 \quad (20c)$$

$$\text{BnGa: } E_{\text{lab}} \leq 2.50 \text{ GeV and } L \leq 9. \quad (20d)$$

We will now evaluate the RHS of the sum rule at fixed t defined by¹

$$S_i^{(\sigma)}(t, k) = \pi B_i^{(\sigma)} \frac{\nu_M^k}{\Lambda^{k+1}} + \int_{\nu_0}^{\Lambda} \text{Im} A_i^{(\sigma)}(\nu, t) \nu^k \frac{d\nu}{\Lambda^{k+1}}, \quad (21)$$

at 11 equally spaced points in the range $t \in [-1, 0] \text{ GeV}^2$. The region of integration is indicated in Fig. 2. There is a

region outside the physical region in which the amplitude requires an extrapolation. In the unphysical region the cosine of the scattering angle reaches unphysical values $\cos \theta < -1$. But since the partial wave analyses are performed at the level of multipoles, the $\cos \theta$ dependence is polynomial and given explicitly by Legendre polynomials. For high angular momentum in the multipole expansion, numerical overflow could appear as the expansion goes as $(\cos \theta)^{L_{\text{max}}}$. We have checked that the SAID and MAID scalar functions for all isospin components are continuous in the unphysical region when we use the complete model available online, *i.e.* $L_{\text{max}} = 5$.

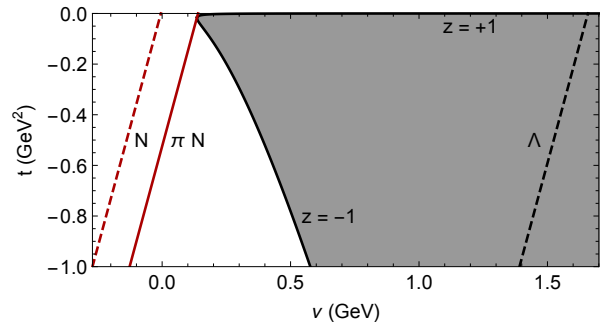


FIG. 2. Region under investigation in this work in the $t - \nu$ plane. For fixed value of t , the integration region in ν is indicated by the red solid line (the $\pi - N$ threshold) and the black dashed line (the cutoff). The physical region of the process $\gamma N \rightarrow \pi N$ is indicated by the gray shaded area, limited by $z = \cos \theta = \pm 1$.

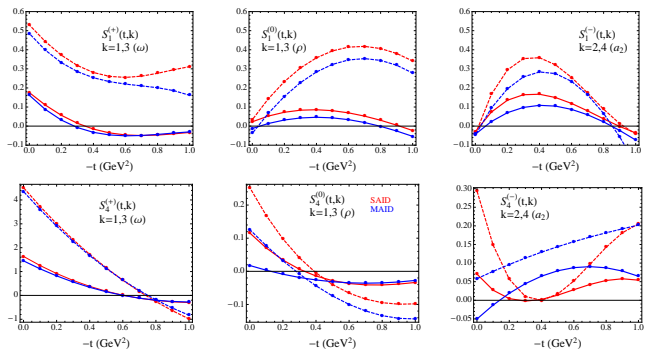


FIG. 3. First moments of the RHS of the FESR Eq. (21) for $A_{1,4}^{(0,+,-)}$ with SAID and MAID models. The lowest spin particle on the corresponding Regge trajectory is indicated for convenience. The dashed (solid) lines correspond to the moment $k = 1$ or $k = 2$ ($k = 3$ or $k = 4$).

The quantity in Eq. (21), corresponding to the LHS of the FESR, is presented in Figs 3 and 4 for all isospin components and the first two moments ($k = 1, 3$ for the crossing-even amplitudes and $k = 2, 4$ for the crossing-odd amplitudes). We choose $E_{\text{lab}}^{\text{max}} = 1.66 \text{ GeV}$ ($W = 2 \text{ GeV}$) corresponding to the end of the domain of the MAID model. The cut-off in Eq. (21) is then, for fixed

¹ We will use the notation $S_2^{(\sigma)}$ for the sum rules performed with $A_2^{(\sigma)}$.

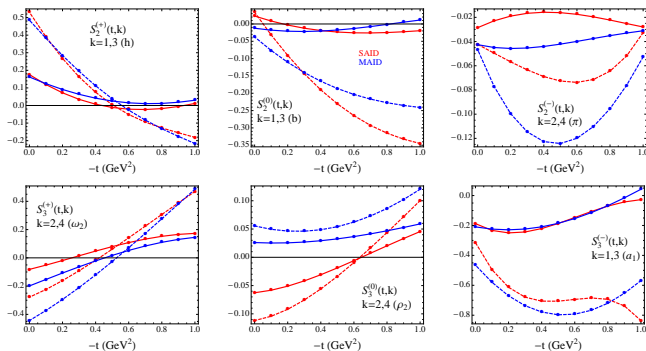


FIG. 4. First moments of the RHS of the FESR Eq. (21) for $A_{2,3}^{(0,+,-)}$ with SAID, MAID models. The lowest spin particle on the corresponding Regge trajectory is indicated for convenience. The dashed (solid) lines correspond to the moment $k = 1$ or $k = 2$ ($k = 3$ or $k = 4$).

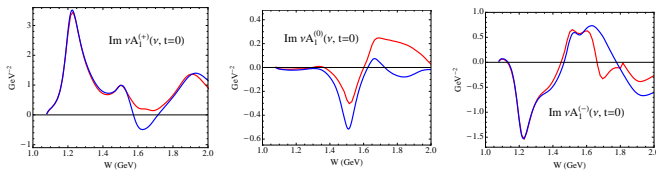


FIG. 5. The SAID and MAID invariant amplitude $\nu A_1^{(0,\pm)}$ at $t = 0$. The Δ resonance is responsible for the non vanishing $S_1^{(0)}(t = 0, k)$.

value of t ,

$$\Lambda \equiv \Lambda(t) = E_{\text{lab}}^{\text{max}} + \frac{t - \mu^2}{4M_N}. \quad (22)$$

According to Eq. (19), the quantity $S_i^{(\sigma)}(t, k)$ is proportional to the residue $\beta_i^{(\sigma)}(t)$ in the hypothesis of a single Regge pole contribution. It is therefore instructive to compare the prediction for these residues from the low energy models and the expectation from Regge theory. For Figs 3 and 4 we observe the following features:

1. The FESR for $A_1^{(0,-)}$ satisfy in good approximation the factorization theorem of Regge pole residues, *i.e.* they are to be proportional to t near the forward direction. However, we observe significant a deviation from factorization in $A_1^{(+)}$. The same deviation appears for the same amplitude in η photoproduction [34]. In Fig. 5, we observe that the strong Δ peak is responsible for the main contribution of $A_1^{(0)}$ at $t = 0$. In the other isospin amplitudes $A_1^{(+)}$ and $A_1^{(-)}$ the baryon resonances cancel to yield $S_1^{(\pm)}(t = 0, k) \approx 0$.
2. The quantities $S_i^{(0,-)}(t, k)$ present a zero at $t \sim -0.8 \text{ GeV}^2$, significantly away from the expected position of the zero of the trajectory $t \sim -0.5 \text{ GeV}^2$. A zero in the residue $\beta_1^{(-)}(t)$ is indeed

expected to cancel the unwanted pole at $\alpha(t \sim -0.5 \text{ GeV}^2) = 0$. Such a zero is called a nonsense wrong signature zero (NWSZ) [37]. This zero might be shifted by the addition of another contribution (a daughter trajectory or a Regge cut) in the sum rules. A non linear trajectory with a zero at $t \sim -0.8 \text{ GeV}^2$ would also explain this observation. The zero in $S_i^{(0)}(t, k)$ can be explained by invoking the degeneracy between the ρ and a_2 Regge poles. The absence of resonances in pp scattering is responsible for the degeneracy of the ρ and a_2 trajectories and nucleon couplings (while their photocouplings are *a priori* unrelated). A zero in the a_2 nucleon coupling would be therefore also present in the ρ nucleon coupling.

3. There are zeros in $S_4^{(0,-)}(t, k)$ at smaller values $t \sim -0.3 \text{ GeV}^2$. The natural explanation is identical to the one in $S_1^{(0,-)}(t, k)$: a NWSZ in the a_2 nucleon coupling reflected in the ρ coupling by degeneracy. However, in this case, the zero appears shifted toward smaller t values. The comparison between $S_4^{(0,-)}(t, k)$ and $S_1^{(0,-)}(t, k)$ then rules out the explanation invoking a non linear trajectory as their zeros appear at different t . We note also that the MAID models do not produce a zero. It would be interesting to investigate the cancellation between resonances producing (or not) this zero in the MAID and SAID approaches.
4. At high energies, the dominant amplitude is $A_4^{(+)}$. The non-flip nucleon couplings of isoscalar trajectories are known to be greater than for isovector exchanges. Moreover in photoproduction there is an additional relative factor of 3 at the photon vertex between isoscalar and isovector exchanges. It is therefore not surprising to observe that $S_4^{(0)}$ is an order of magnitude larger than the other amplitudes. It comes from to the dominant Δ peak. Interestingly enough, $S_4^{(0)}$ presents a zero at large $|t|$. The zero is around $t = -0.75 \text{ GeV}^2$ for the lowest moment and moves to $t = -0.6 \text{ GeV}^2$ for $k = 3$. This zero is certainly related to the dip in the differential cross section for the neutral pion photoproduction. It is usually interpreted as NWSZ although it is not necessary in odd signature Regge poles, *i.e.* there is no ghost pole at $\alpha = 0$ thanks to the signature factor.
5. The factorization of Regge residues appears to be satisfied in good approximation also in $S_2^{(0)}$. However, for $S_1^{(+)}$ and $S_2^{(+)}$ it deviates significantly from the expectation $S_2^{(+)} \propto t$, since $A_2' = A_1 + tA_2$ and the Δ peak in $A_1^{(0)}$ is also responsible for the non zero $S_2^{(+)}$ at $t = 0$. We note also that the pion exchange amplitudes $S_2^{(-)}$ do not vanish in the forward direction as expected from the forward peak

in the photoproduction of a charged pion.

- The exchanges ω_2 and ρ_2 contributing to the amplitudes $A_3^{(0,+)}$ are poorly known and generally assumed to be small. This is consistent with the high energy data, as we will see, that do not favor a large A_3 contribution. This is in contrast with the significantly non zero $S_3^{(0,+)}$. It would be interesting to find the origin of the large $S_3^{(0,+)}$ in the baryon spectrum.

The LHS of the sum rules $S_i^{(\sigma)}$ computed with the SAID and MAID models are generally in agreement in both magnitude and t -dependence. We note however significant difference between SAID and MAID models in magnitude and/or t -dependence in $S_4^{(-)}$, $S_2^{(-)}$ and $S_3^{(0)}$. These moments are quite small compared to the other amplitudes. It is then interesting to note that the small differences between models are magnified in these sum rules. For instance the differences in the moment $S_3^{(0)}(t, k)$ come from the overall shift between the $A_3^{(0)}$ computed with the two models. This is illustrated in Fig. 6.

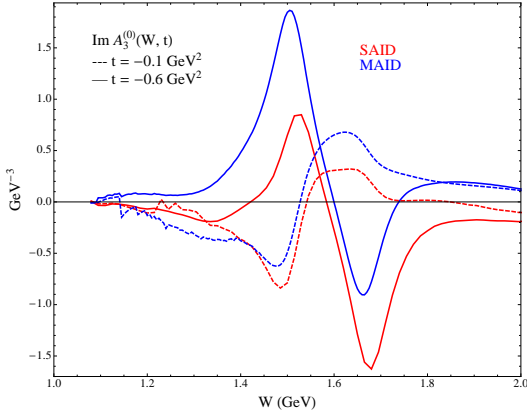


FIG. 6. Imaginary part of the scalar amplitudes $A_3^{(0)}(W, t)$ at $t = -0.1 \text{ GeV}^2$ and $t = -0.6 \text{ GeV}^2$ computed with the SAID and MAID models.

The advantage of the CGLN basis is the simple relation between the scalar functions A_i and the leading s -channel helicity amplitudes in Eq. (9). The t factor from the factorization properties of Regge poles are readily checked thanks to Eq. (10). Since the scalar functions have also good t -channel quantum numbers and the magnitudes of the s -channel nucleon couplings are known for all exchanges [9] we could deduce the expected relative strength of the $S_i^{(\sigma)}$. The pattern of zeros displayed in $S_i^{(\sigma)}$ is instructive as, in the single Regge pole approximation, it connects directly to the zeros in the high energy s -channel amplitudes and hence in the high energy observables. The properties of Reggeons are also best described in their rest-frame, the t -channel. For

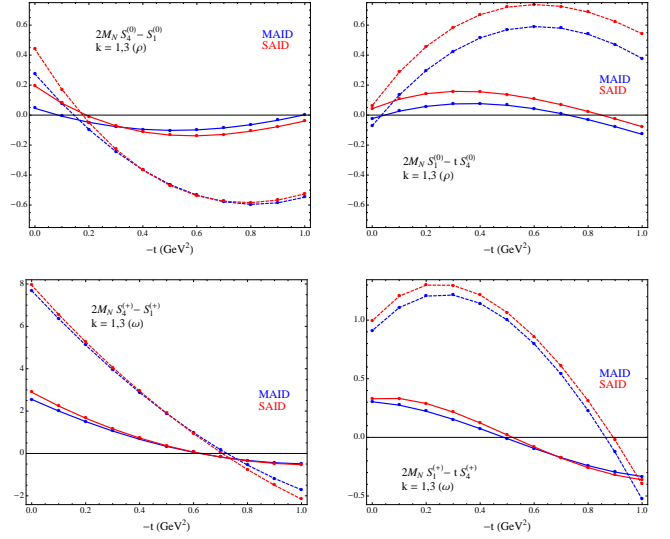


FIG. 7. t -channel invariant amplitudes $F_1^{(0,+)}$ and $F_3^{(0,+)}$, Eq. (23), with the MAID and SAID models. The solid (dashed) lines are $k = 3$ ($k = 1$).

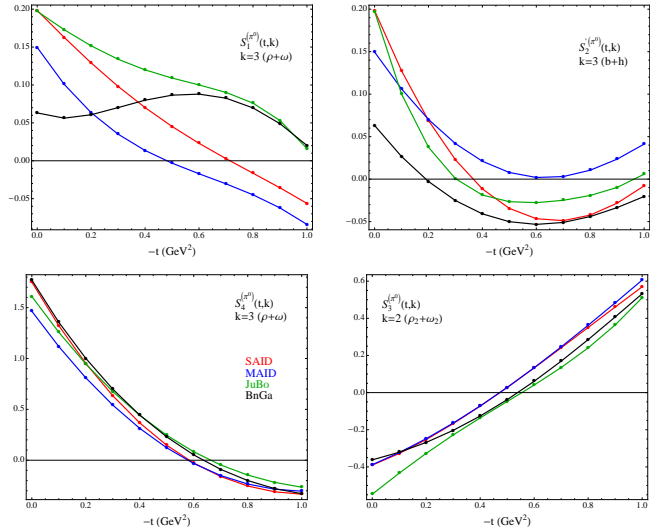


FIG. 8. Lowest moments of the RHS of the FESR Eq. (21) for $A_i^{(\pi^0)} = A_i^{(0)} + A_i^{(+)}$ with SAID, MAID and JüBo ($L_{\max} = 5$ is used) solutions for the process $\gamma p \rightarrow \pi^0 p$. The lowest spin particle on the corresponding Regge trajectories are indicated for convenience. The dashed (solid) lines correspond to the moment $k = 1$ or $k = 2$ ($k = 3$ or $k = 4$).

natural exchanges the relevant combinations are

$$F_1 = -A_1 + 2M_N A_4, \quad (23a)$$

$$F_3 = 2M_N A_1 - t A_4. \quad (23b)$$

F_1 (F_3) is nucleon helicity non-flip (flip) in the t -channel [20]. We now wish to compare the features of the ρ and ω Regge poles obtained by the FESR in other reactions. For this purpose we perform the appropriate combination of $S_i^{(\sigma)}$, from Eq. (23), and compare

to the same quantities in $\gamma p \rightarrow \eta p$, Fig. 8 of Ref. [34], and $\pi p \rightarrow \pi p$, Fig. 2 of Ref. [35]. Our result is presented in Fig. 7. We note a striking similarity between the pion and eta meson photoproduction for the ω exchange. The sum rules for the (t -channel) nucleon non-flip combination F_1 displays in both cases a zero for $t \sim -0.6$ GeV². The sum rules for (t -channel) nucleon flip combination F_3 displays in both cases a violation of factorization and a zero for $t \sim -0.5$ GeV². The factorization of the ρ pole residues is observed in both pion and eta meson photoproduction for the nucleon flip combination but a zero appears for the moment $k = 3$ only in pion photoproduction. This zero is a bit shifted compared to the nucleon flip amplitudes for pion-nucleon scattering. The zero appears at $t \sim -0.8$ GeV² for pion photoproduction and at $t \sim -0.5$ GeV² for pion-nucleon scattering. In the ρ nucleon non-flip combination, the zero appears at the same location $t \sim -0.15$ GeV² in both reactions. This zero was responsible for the cross-over between $\pi^- p$ and $\pi^+ p$ elastic scatterings [35]. All these observations suggest that the zeros in the Regge residues would come from the nucleon vertex, as it is the common piece in all these reactions.

It is worth mentioning that we do not possess any information about the error of the models presented. The neutron target data set being smaller than the proton target one, it would be interesting to observe the effect of the recent data from CLAS on neutron target [45], currently under investigation by the different groups, on the isospin amplitudes $A_i^{(\sigma)}$.

For completeness we wish to compare the FESR obtained with the JüBo and BnGa models² with the SAID and MAID models. The JüBo and BnGa model is only available for reactions on a proton target. We can only present the results for the process $\gamma p \rightarrow \pi^0 p$ since the process $\gamma p \rightarrow \pi^+ n$ does not have good properties under crossing symmetry (its u -channel discontinuity is given by the s -channel discontinuity of $\gamma n \rightarrow \pi^- p$). The comparison between JüBo, BnGa, SAID and MAID models is presented in Fig. 8. The cutoff $E_{\text{lab}} = 1.66$ GeV ($\sqrt{s} = 2$ GeV) is used in the FESR and only the moment $k = 2$ or $k = 3$ is presented. The JüBo and BnGa models compare very well with the SAID and MAID solutions except for $S_1^{(\pi^0)} = S_1^{(0)} + S_1^{(+)}$.

We can identify the cause of this difference by looking at the invariant amplitudes at fixed t . We compare in Fig. 9, the four scalar functions for the neutral pion photoproduction reconstructed from the SAID, MAID, BnGa and JüBo multipoles, as a function of the energy at $t = -0.2$ GeV². We note that all models compare well, except for the A_1 amplitude in the unphysical region (marked by the dashed line in the figure). Again it is

interesting to note that the FESR can amplify the small differences between the various analysis. **Here a word on ANL-O when I'll receive multipoles from Toru Sato.**

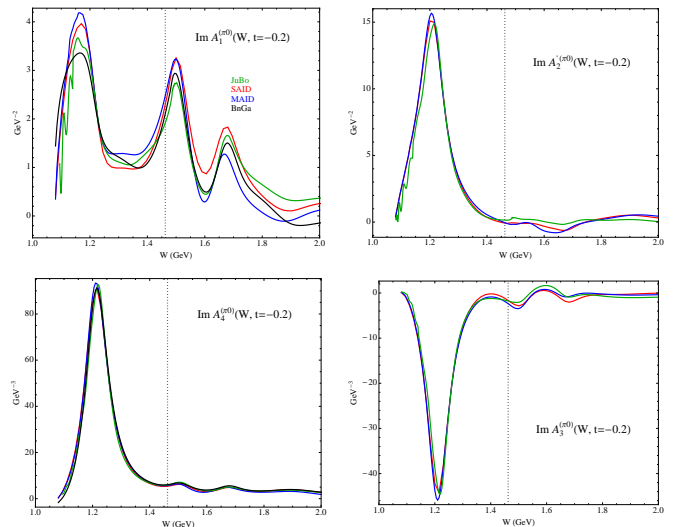


FIG. 9. The invariant amplitudes A_i with SAID, MAID, BnGa ($L_{\text{max}} = 5$ is used) and JüBo solutions for the process $\gamma p \rightarrow \pi^0 p$ at $t = -0.2$ GeV². The beginning of the physical region is indicated by the vertical black dashed line.

V. REGGE RESIDUES FROM FESR

From the FESR, Eq. (19), we can test if the amplitudes are dominated by only one single Regge pole. Indeed, if the LHS of the FESR in Eq. (19) involves only one Regge pole, the combination (with Λ expressed in GeV)

$$\widehat{\beta}_i^{(\sigma)}(t) = S_i^{(\sigma)}(t, k) \frac{\alpha_i^{(\sigma)}(t) + k}{\Lambda \alpha_i^{(\sigma)}(t) - 1}, \quad (24)$$

should be independent of the moment k (the Λ dependence in the effective residue is understood). The calculation of the Regge residues from the low energy model requires the knowledge of the trajectories $\alpha_i^{(\sigma)}(t)$. We shall assume that the natural exchanges trajectories ρ, ω, a_2 are exchange degenerate (EXD) [46]. We shall assume also EXD between the unnatural exchanges π, b, h, a_1 trajectories:

$$\alpha_{1,4}^{(\sigma)} \equiv \alpha_N(t) = 0.9(t - m_\rho^2) + 1 \quad \sigma = \{0, +, -\} \quad (25a)$$

$$\alpha_{2,3}^{(\sigma)} \equiv \alpha_U(t) = 0.7(t - m_\pi^2) + 0 \quad \sigma = \{0, +, -\}. \quad (25b)$$

The trajectories Eq. (25) are compared to the meson masses in Fig. 10. All masses are taken from the Review of Particle Physics (RPP) [33], except for the ρ_2 and ρ_4 . There is no experimental evidence for the ρ_2 and ω_2 mesons. However, one could take the quark model predictions to estimate their masses. In Fig. 10 we take the

² We use the latest version of the BnGa to be published soon. We thank A. Sarantsev for providing us with their new multipoles prior to their publication.

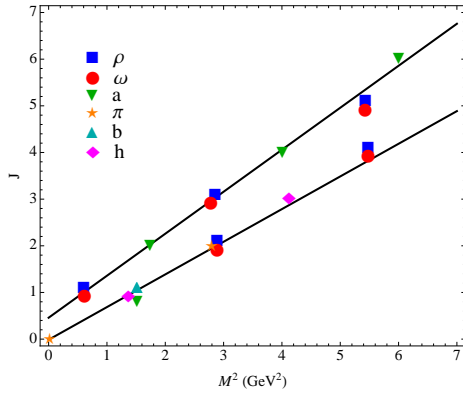


FIG. 10. Chew-Frautchi plot for natural and unnatural parity mesons. The solid lines indicate the two Regge trajectories α_N and α_U in Eq. (25) used in this work.

mass of the ω_2/ρ_2 and ω_4/ρ_4 from the quark model predictions of Godfrey and Isgur [47] (the isoscalar mesons are degenerated with the isovector in this model). In the production region $t > 0$, all natural mesons are aligned with the trajectory $\alpha_N(t)$. The same degeneracy appears for the unnatural mesons and $\alpha_U(t)$, including the quark model predictions for the 2^{--} and 4^{--} mesons. Accordingly, we shall use $\alpha_U(t)$ for the trajectory to extract $\widehat{\beta}_3^{(0,+)}$.

In Figs 11 and 12 we show the effective residues $\widehat{\beta}_i^{(\sigma)}$ computed with Eq. (24) using the cutoff $E_{\text{lab}} = 2$ GeV and the SAID model. To test the dominance of a single Regge pole we show the first four moments. In all 12 amplitudes, the extracted residues are almost independent of k . We note however that the moment $k = 1$ is sometimes different from the other moments. This might be due to the stronger influence of the unphysical region in the lowest moment. We have checked that the effective residues are also approximately independent of the moment (except for the lowest one) also with the MAID models. The effective residues extracted with the MAID model are presented in Figs 13 and 14.

The dominance of one single Regge pole in each amplitude, with the trajectories (25), is then satisfied in a very good approximation. In the absence of errors in the SAID and MAID models, we cannot make a statement on the origin of the slight differences between different moments. They could lie within the uncertainty of the low energy model or come from the sensibility to the unphysical region and/or originate from corrections (Regge cut and daughter trajectories) beyond the single pole approximation. These latter two effects are indeed suppressed by taking higher moments.

As we mentioned above the ghost pole in the a_2 (even signature) amplitude should be cancelled by a zero in the residue. This zero is expected around $t = -0.5$ GeV². This zero does not appear, except in $\widehat{\beta}_4^{(-)}$ with the SAID model. The absence of a zero in $\widehat{\beta}_1^{(-)}$ suggests a strong correction to the Regge pole approximation. However

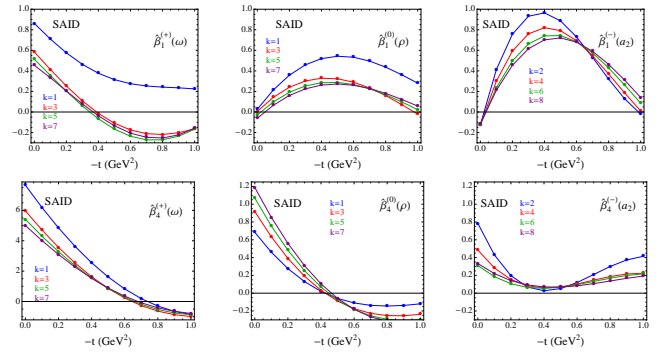


FIG. 11. Residue extracted from the RHS of the FESR Eq. (24) for $A_{1,4}^{(0,+,-)}$ with the SAID model calculated with $E_{\text{lab}}^{\text{max}} = 2.0$ GeV. The lowest spin particle on the corresponding Regge trajectory is indicated for convenience.

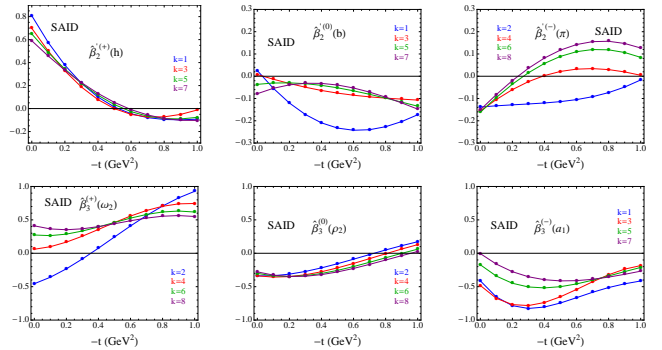


FIG. 12. Residue extracted from the RHS of the FESR Eq. (24) for $A_{2,3}^{(0,+,-)}$ with the SAID model calculated with $E_{\text{lab}}^{\text{max}} = 2.0$ GeV. The lowest spin particle on the corresponding Regge trajectory is indicated for convenience.

the almost k independence of the effective residues suggests that the RHS of the sum rules is saturated by only one term. We do not have a solution for this apparent paradox.

Since the Regge trajectories are fairly well given empirically by Eq. (25), we have not studied the dependence of the effective residues in the trajectories α_N and α_U . The validity of the SAID model extends to $E_{\text{lab}} = 2.4$ GeV. In our analysis of πN scatterings [35], we found a good agreement between both sides of the sum rules for $E_{\text{lab}}^{\text{max}} > 2.0$ GeV. Using the SAID model we can study the evolution of the residues $\widehat{\beta}_i^{(\sigma)}$ as the cutoff varies. We display $\widehat{\beta}_i^{(\sigma)}$ for $k = 3$ (or $k = 2$ for odd amplitudes) for $E_{\text{lab}}^{\text{max}} = 1.7, 2.0$ and 2.3 GeV in Fig. 15. We observe a cutoff dependence in the effective residues but the main features remain the same in the range $E_{\text{lab}}^{\text{max}} = 1.7 - 2.3$ GeV.

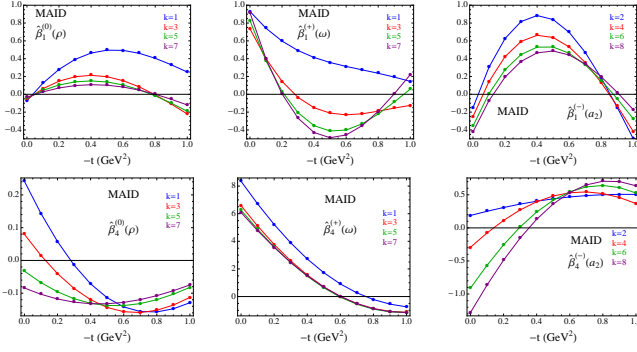


FIG. 13. Residue extracted from the RHS of the FESR Eq. (24) for $A_{1,4}^{(0,+,-)}$ with the MAID model. The lowest spin particle on the corresponding Regge trajectory is indicated for convenience.

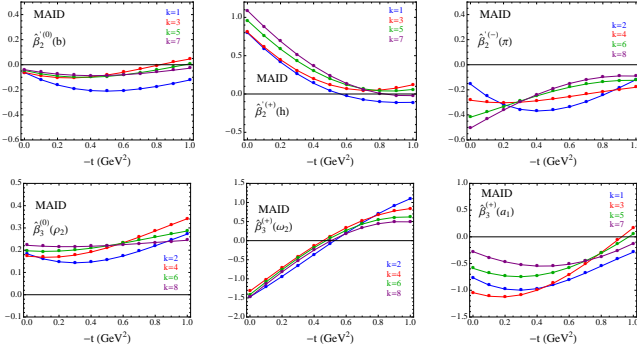


FIG. 14. Residue extracted from the RHS of the FESR Eq. (24) for $A_{2,3}^{(0,+,-)}$ with the MAID model. The lowest spin particle on the corresponding Regge trajectory is indicated for convenience.

VI. HIGH ENERGY PREDICTIONS FROM FESR

With the SAID model displaying nearly moment independence of the extracted residues, it is interesting to investigate the predictions of the SAID model for the observables in the Regge region. With this aim, we reconstruct the invariant amplitudes from the extracted residues $\hat{\beta}_i(t)$:

$$\hat{A}_i^{(\sigma)} = -\hat{\beta}_i^{(\sigma)}(t) \frac{\tau_i^{(\sigma)} + e^{-i\pi\alpha_i^{(\sigma)}(t)}}{\sin \pi\alpha_i^{(\sigma)}(t)} \nu^{\alpha_i^{(\sigma)}(t)-1}. \quad (26)$$

The trajectories $\alpha_i^{(\sigma)}(t)$ are given by Eq. (25) and the residues $\hat{\beta}_i^{(\sigma)}(t)$ by Eq. (24). Note that ν has to be expressed in GeV since in the calculation of the residues with Eq. (24), Λ was expressed in GeV.

We have seen in the previous section that the a_2 pole residues $\hat{\beta}_{1,4}^{(-)}$ do not incorporate the expected zero at $\alpha_N(t) = 0$, *i.e.* $t \sim -0.5 \text{ GeV}^2$. Thus the amplitudes $\hat{A}_{1,4}^{(-)}$ reconstructed in this way will have an unwanted pole at $t \sim -0.5 \text{ GeV}^2$. This prevents us from making

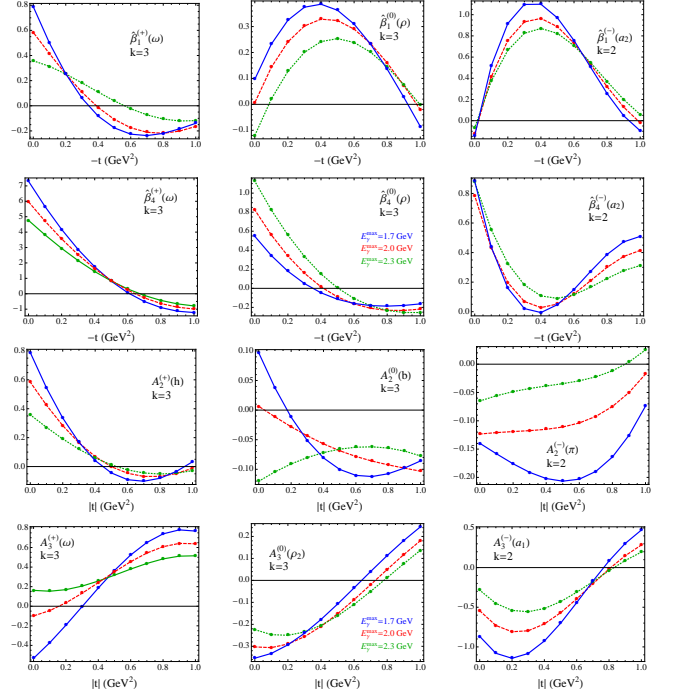


FIG. 15. Cutoff dependence of the LHS of the FESR with the SAID models. Only the moments $k = 4$ (odd amplitudes) or $k = 5$ (even amplitudes) are displayed. The chosen maximal energy of the beam in lab frame $E_{\text{max}}^{\gamma} = 1.26, 1.66, 2.11 \text{ GeV}$ correspond to $\sqrt{s} = 1.8, 2.0, 2.2 \text{ GeV}$.

any reliable predictions involving these scalar amplitudes. We then focus only on the prediction for neutral pion photoproduction.

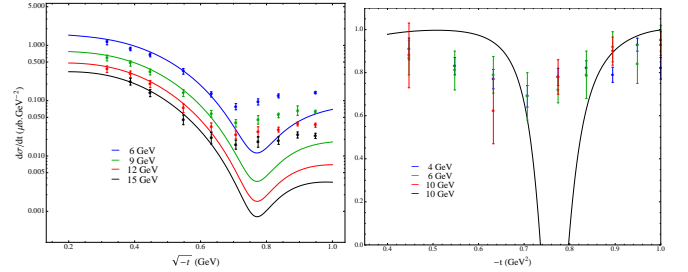


FIG. 16. Prediction for differential cross section and beam asymmetry for $\gamma p \rightarrow \pi^0 p$ using the reconstructed scalar amplitudes from Eq. (26).

Fig. 16 shows the comparison between the data from Ref. [48] and the prediction

$$\frac{d\hat{\sigma}}{dt} = \frac{(\hbar c)^2}{32\pi} \left[\left| \hat{A}_1^{\pi^0} \right|^2 - t \left| \hat{A}_4^{\pi^0} \right|^2 + \left| \hat{A}_2^{\pi^0} \right|^2 - t \left| \hat{A}_3^{\pi^0} \right|^2 \right], \quad (27)$$

where $\hat{A}_i^{\pi^0} = \hat{A}_i^{(+)} + \hat{A}_i^{(0)}$. According to the discussion in the previous section, we discard the effective residues with $k = 1$. We have calculated the prediction using the $k = 3$ moment for the residues $\hat{\beta}_i^{(\sigma)}(t)$. Other moments

yield similar results since the effective residues are almost k -independent for $k > 1$.

The overall magnitude of the differential cross section is driven by the dominant ω exchange amplitudes $A_4^{(+)}$. For a better comparison with the data, we changed slightly the intercept of the natural exchange trajectories and used $\alpha_N(t) - 0.15 = 0.31 + 0.9t$ in the Fig. 16. This changes amounts to reduce the residues by 65%. When we will perform a global fit, it will be therefore not surprising to obtain an intercept for the ω trajectory somewhat lower than expected.

With this little change, the prediction is in very good agreement with the data in the forward region $-t \leq 0.4$ GeV. The energy dependence is, of course, coming from the trajectories that are inserted by hand, *i.e.* not coming from the LHS of the sum rules but the overall agreement in shape is very nice in the forward direction. The discrepancy at larger $-t$ is not surprising since Regge cuts, not considered in this prediction, are needed to describe properly the data [20] for $|t| > 0.5$ GeV². It is nevertheless impressive to see that a model in the low energy region can actually make a reliable prediction for the high energy and forward angles!

The overall normalization, important for the differential cross section, should play a less significant role in the beam asymmetry Σ . The latter, expressed by the ratio

$$\widehat{\Sigma} = \frac{|\widehat{A}_1^{\pi^0}|^2 - t|\widehat{A}_4^{\pi^0}|^2 - |\widehat{A}_2^{\pi^0}|^2 + t|\widehat{A}_3^{\pi^0}|^2}{|\widehat{A}_1^{\pi^0}|^2 - t|\widehat{A}_4^{\pi^0}|^2 + |\widehat{A}_2^{\pi^0}|^2 - t|\widehat{A}_3^{\pi^0}|^2}, \quad (28)$$

is sensitive to the ratio of unnatural and natural exchanges. Since the differential cross section, dominated by the natural exchange, proved that the natural exchange has the correct t -dependence, the beam asymmetry provides indication about the t -dependence of the unnatural exchange amplitudes A_2' and A_3 .

The prediction for the beam asymmetry is essentially flat and close to 1 at forward angles. The strong dip at $-t \sim 0.6$ GeV² is of course related to the zero of the dominant residue $\widehat{\beta}_4^{(0)}$. As we mentioned the Regge cuts traditionally invoked to fill this dip are not considered in this prediction. In view of the beautiful agreement for the differential cross section, we expected a better agreement in the forward direction $|t| < 0.4$ GeV² for the beam asymmetry. This shows that the t -dependence of FESR for the unnatural amplitudes might need improvement. It would be interesting to investigate which resonances influence more the t -dependence of the unnatural amplitudes.

We do not present the prediction for the target and recoil polarization as they are zero in the single Regge pole approximation. As is well known the non-zero target and recoil asymmetries at high energies suggest corrections to the leading Regge pole approximation.

VII. COMBINED FIT OF THE FESR AND OBSERVABLES

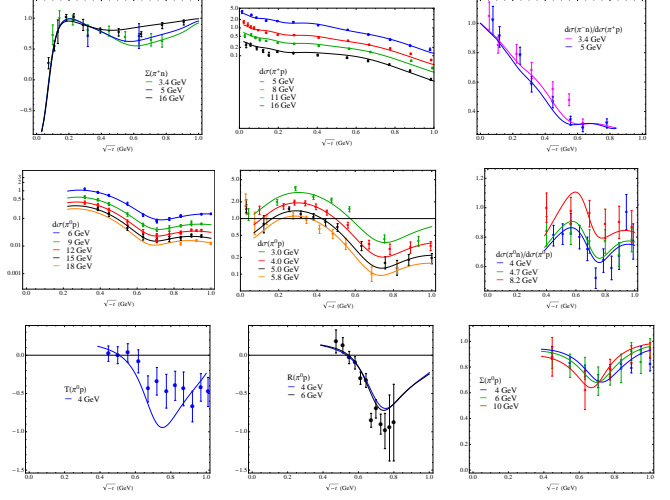


FIG. 17. Comparison between the model given by Eq. (29) and Tables III and IV and the observables.

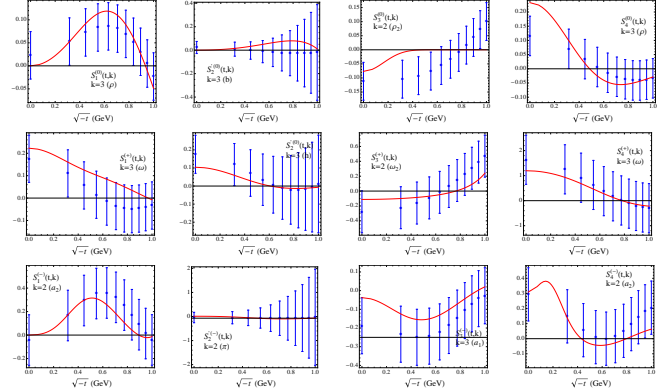


FIG. 18. Comparison between the model given by Eq. (29) and Tables III and IV and the FESR using the SAID model. The band is the uncertainty used in the fit and equal to 60% of the maximum value.

In the previous section we showed that the LHS of the sum rules, $S_i^{(\sigma)}(t, k)$, suggested the dominance of a leading Regge pole in each of the 12 isospin scalar amplitudes. The extraction of an effective residue for these leading trajectories yielded reasonable predictions for the high energy observables but nevertheless suggested corrections to the leading Regge pole approximation. In this section we continue our analysis by fitting jointly the FESR $S_i^{(\sigma)}(t, k)$ and the high energy observables.

For the high energy observables we restrict the data set to the kinematical region $E_{\text{lab}} \geq 3$ GeV and $-t \geq 1$ GeV². In this region we have the following data sets:

- Differential cross section for $\gamma p \rightarrow \pi^0 p$ from Refs [48–51].

- Ratio of differential cross section $\gamma n \rightarrow \pi^0 n$ over proton target from Refs [52] and [53].
- $\gamma p \rightarrow \pi^0 p$ beam [54], target [55] and recoil asymmetry [56].
- Differential cross section for $\gamma p \rightarrow \pi^+ n$ from Refs [57], [58], [59] and [60].
- Ratio of differential cross sections $\gamma n \rightarrow \pi^- p$ over $\gamma p \rightarrow \pi^+ n$ from Ref. [61].
- $\gamma p \rightarrow \pi^+ p$ beam asymmetry from [62].

In order to enhance the small t region, where the pion exchange dominates the $\gamma p \rightarrow \pi^+ n$ differential cross section all the figures in this section are plotted with respect to $\sqrt{-t}$.

Since we do not have any information about the uncertainty of the LHS of the sum rules, we generated the errors artificially. We used the $S_i^{(\sigma)}(t, k)$ derived from the SAID model with the cutoff $E_{\text{lab}}^{\text{max}} = 1.66$ GeV ($W = 2.0$ GeV) for the $k = 2$ or $k = 3$ moments. The uncertainty, used in the fit, is taken as 60% of the maximal values (for each scalar amplitude) and taken constant for all t . Note that since $A'_2 = A_1 + tA_2$, the uncertainty on A'_2 grows linearly with t .

In order to properly describe the observables and the LHS of the sum rules $S_i^{(\sigma)}(t, k)$, our models for the imaginary part of the scalar amplitudes involve a summation of Regge poles-like terms:

$$\text{Im } A_i^{(\sigma)}(\nu, t) = \sum_j \beta_{ij}^{(\sigma)}(t) \nu^{\alpha_j(t)-1}. \quad (29)$$

Equating the left and right hand sides of the sum rules, this form yields, with $\Lambda = E_{\text{lab}}^{\text{max}} + (t - \mu^2)/(4M_N)$,

$$S_i^{(\sigma)}(t, k) = \sum_j \beta_{ij}^{(\sigma)}(t) \frac{\Lambda^{\alpha_j(t)-1}}{\alpha_j(t) + k}. \quad (30)$$

Note that we use the expression (29) to fit $A'_2^{(\sigma)}$, *i.e.* in the formula (29) the index $i = 2$ stand for the amplitudes $A_2^{(\sigma)}$. In each amplitude the summation involves at least one term representing the leading Regge pole contribution. The parameters of the trajectories $\alpha_j(t) = \alpha_j^0 + \alpha_j^1 t$ of these first terms are constrained to lie in the interval around the expected values in Eq. (25). When necessary to describe the data and the LHS of the sum rules, we add a second term. These corrections are parametrized as a pole contribution but the parameters of their trajectories are unconstrained. The trajectory parameters and interpretation are summarized in Table III.

Since all $S_i^{(\sigma)}(t, k)$ have only one extremum, we parametrize the residues with a second order polynomial and an exponential fall-off. The residues are (omitting the indices (σ) and ij)

$$\beta(t) = \alpha^\kappa(t) t^\delta \times \beta_0 e^{bt} (1 - \gamma_1 t)(1 - \gamma_2 t). \quad (31)$$

TABLE III. Solution of the fit for the trajectories.

j	α_j^0	α_j^1 (GeV ⁻²)	role
1	0.541	0.711	ρ pole
2	0.316	0.897	ω pole
3	0.699	1.100	a_2 pole
4	0.401	0.661	ρ/ω pole/cut
5	-0.010	1.00	a_2 cut
6	-0.007	0.615	π, b, h, a_1 pole
7	1.031	1.770	ρ_2, ω_2 pole
8	0.197	0.330	ω cut

The first factor $\alpha_j^\kappa(t)$ is need only in the $A_{1,4}^{(-)}$ and $A_3^{(0,+)}$ amplitudes. Since they involve the the even trajectories a_2, ρ_2 and ω_2 . This factor cancels the unwanted ghost pole at $\alpha_j(t) = 0$ that might appear in the physical region. Indeed the even signature amplitudes $A_{1,2,4}^{(-)}$ and $A_3^{(0,+)}$ have the form

$$A_i^{(\sigma)}(\nu, t) = \sum_j \beta_{ij}^{(\sigma)}(t) \nu^{\alpha_j(t)-1} \left[i - \cot \frac{\pi}{2} \alpha_j(t) \right] \quad (32)$$

and have a pole at $\alpha_j(t) = 0$. Note that we did not need this factor in the π exchange amplitudes $A_2^{(-)}$ since we expect the point $\alpha_\pi(t = m_\pi^2) = 0$ to lie outside the fitting region $t < 0$. Our fit, cf. Table III, led to $\alpha_6(t) = 0$ at $\sqrt{t} = 0.107$ GeV close to the pion mass (and outside the fitting region). For completeness we quote the full expression for the odd signature amplitudes, $A_{1,2,4}^{(0,+)}$ and $A_3^{(-)}$:

$$A_i^{(\sigma)}(\nu, t) = \sum_j \beta_{ij}^{(\sigma)}(t) \nu^{\alpha_j(t)-1} \left[i + \tan \frac{\pi}{2} \alpha_j(t) \right]. \quad (33)$$

The second factor t^δ in Eq. (31) imposes factorization in the A_1 and A'_2 amplitudes. As can be seen in Table III, the poles in these amplitudes are forced to have a factorisable form, except for the pion pole. It is necessary to have a finite residue for the pion pole in order to describe the forward peak in the charged pion photoproduction. The h pole in $A_2^{(+)}$ does not have the t factor either as the FESR suggests a significant deviation from factorization. The deviation from factorization in the $A_1^{(+)}$ amplitude is modeled by a cut correction $j = 8$. The ω pole $j = 1$ in this amplitude has the factor t imposed.

Using the model for the residues described above we now fit both the FESR and the observables. The 12 $S_i^{(\sigma)}(t, k)$ provide independent and linear constraints on the imaginary part of the scalar amplitudes. They are computed at 11 equally spaced t in the region $-1 > t/\text{GeV}^2 > 0$. The observables are non independent and quadratic constraints on the scalar amplitudes. We wish to isolate subsets of observables sensitive only to subsets of exchanges. The fit is therefore performed step by step.

TABLE IV. Results of the fit for the residues Eq. (31).

	κ	δ	β_0	b	γ_1	γ_2	
ρ	$\beta_{11}^{(0)}$	0	1	0.787	1.933	5.131	4.008
	$\beta_{14}^{(0)}$	0	1	-3.418	1.942	2.47	0.928
ω	$\beta_{12}^{(+)}$	0	1	6.657	3.655	0.023	-0.37
	$\beta_{18}^{(+)}$	0	0	1.068	2.029	-0.842	5.401
a_2	$\beta_{13}^{(-)}$	1	1	-2.361	1.437	-0.936	3.939
	$\beta_{15}^{(-)}$	1	1	80.783	7.902	-0.059	0.001
b	$\beta_{26}^{(0)}$	0	1	-0.678	0.431	2.975	-0.975
h	$\beta_{26}^{(+)}$	0	0	0.517	1.680	-2.692	-0.834
π	$\beta_{26}^{(-)}$	0	0	0.035	3.89	-22.95	9.01
ρ_2	$\beta_{37}^{(0)}$	1	0	-0.222	11.366	-2.311	-3.538
ω_2	$\beta_{37}^{(+)}$	1	0	-0.325	0.000	0.491	0.507
a_1	$\beta_{36}^{(-)}$	0	0	-0.186	2.421	37.472	-1.130
ρ	$\beta_{41}^{(0)}$	0	0	-0.507	2.184	5.810	-0.623
	$\beta_{44}^{(0)}$	0	0	1.595	4.639	0.763	-0.033
ω	$\beta_{42}^{(+)}$	0	0	1.911	1.518	0.181	1.459
	$\beta_{44}^{(+)}$	0	0	3.627	2.223	-2.950	1.805
a_2	$\beta_{43}^{(-)}$	1	0	0.726	3.171	-6.418	1.429
	$\beta_{45}^{(-)}$	1	0	-47.357	27.854	1.550	-1.513

The results of our model are compared to the high energy data in Fig. 17 and both sides of the sum rules are displayed in Fig. 18.

We start by fitting the differential cross sections (on proton target and the ratio neutron over proton target) and the target and recoil asymmetries for neutral pion photoproduction with only $A_{1,4}^{(0,+)}$. They are all sensitive to the ω and ρ exchanges. The trajectories of the poles $j = 1$ in $A_{1,4}^{(0)}$ and $j = 2$ in $A_{1,4}^{(0)}$, *i.e.* the ω and ρ poles, are constrained around $\alpha_N(t) = 0.9(t - m_\rho^2)$. A unconstrained cut is added in all these amplitudes. In order to limit the number of parameters, we have tried to use the same cut $j = 4$ in all four amplitudes. However the $A_1^{(0)}$ FESR needed a different cut to describe properly the violation of factorization at $t = 0$. The cut added to these amplitudes is needed to describe the target and recoil asymmetries (they would vanish with only a ρ and an ω pole) but also to reproduce the FESR. We then turn to the unnatural exchanges amplitudes $A_{2,3}^{(0,+)}$, keeping $A_{1,4}^{(0,+)}$ fixed, and fit the neutral pion beam asymmetry (as well as the FESR for $A_{2,3}^{(0,+)}$). The $A_2^{(0,+)}$ contains only the b and the h poles and we impose degeneracy of their trajectories, *i.e.* the only non zero residues are $\beta_{2j}^{(0,+)}$ with $j = 6$. As we mentioned above the pa-

rameters of the trajectory $\alpha_6(t)$ are constrained around $\alpha_U(t) = 0.7(t - m_\pi^2)$.

For the charged pion observables, we fit simultaneously the differential cross sections (on proton target and the ratio neutron over proton target), the beam asymmetry and the $A_{1,2,3,4}^{(0,-)}$ FESR. Since the pion is responsible for the forward peak in the differential cross section, we cannot separate unnatural and natural exchanges easily as we did for the neutral pion fit. For this fit, the initial values for all the parameters related to the ρ amplitudes $A_{1,4}^{(-)}$ are the results obtained for the neutral pion fit. We also impose the initial condition $\gamma_1 = -30$ in the π exchange amplitude $A_2^{(0)}$. Indeed the dominance of the pion exchange in the forward direction and the charged pion beam asymmetry $\Sigma(\sqrt{-t} \sim 0.1 - 0.2) = 1$ suggest a zero in the pion amplitude around $t \sim 0.01 - 0.04 = -1/\gamma_1$. We have used the same pole $j = 6$ in the π and a_1 amplitudes (as well as in the b and h amplitudes) according to the discussion on the degeneracies between trajectories in Sec. V. We have tried to impose the same $j = 6$ pole for the ρ_2 and ω_2 amplitudes $A_3^{(0,-)}$ but we needed more flexibility in the parametrization to describe their FESR and the observables. The $A_3^{(0,-)}$ display significant FESR but the neutral and charged pion beam asymmetries constrain the amount of unnatural exchanges. In order to reproduce these asymmetries, we needed to suppress one of the unnatural amplitudes, which we choose to be the $A_3^{(0)}$. The ρ_2 amplitudes influence both neutral and charged asymmetries. By suggesting a large exponential suppression parameter b in the initial condition we could obtain a good description of the asymmetries and the other unnatural FESR. The cut term $j = 5$ in the $A_{1,4}^{(-)}$ amplitudes is necessary to reproduce the shape of the LHS of the FESR. Indeed the pole term needs to vanish at the zero of the trajectory to remove the ghost pole. With only one common pole, $S_1^{(-)}$ and $S_4^{(-)}$ would have a zero at the same place. Since the zero in $S_1^{(-)}$, around $-t = 0.9 \text{ GeV}^2$ is shifted from the zero in $S_4^{(-)}$, around $-t = 0.4 - 0.8 \text{ GeV}^2$, we needed the cut $j = 5$ to add flexibility in the fit and describe both $S_1^{(-)}$ and $S_4^{(-)}$ properly.

We then performed a global fit of all neutral and charged pion observables and FESR, keeping the parameters of the isoscalar (ω, ω_2 and h) and isovector negative G -parity (a_2, a_1 and π) parameters fixed but fitting the parameters of the isovector positive G -parity (ρ, ρ_2 and b). The final parameters are listed in Table IV.

As expected from our discussion in Sec. VI, the ω pole trajectory $\alpha_2(t) = 0.316 + 0.897t$ is very close to the values we used to match the predictions from the sum rules and the data. The second contribution to the ρ pole, $j = 4$ is difficult to interpret as daughter or a cut as its intercept is similar to a pole. The terms $j = 1$ and $j = 4$ have similar trajectory and are interpreted together as the ρ pole. The origin of the second term $j = 4$ is to provide enough freedom to describe the FESR and the

recoil and target asymmetry in neutral pion photoproduction. The second contributions $j = 5$ and $j = 8$ to the a_2 and ω amplitudes have an intercept of the order of the unnatural pole $j = 6$ intercept. The natural and unnatural amplitudes are then expanded to the same level of approximation $\mathcal{O}(s^0)$.

The number of points in each $S_i(\sigma)$ is arbitrary. We have chosen 11 points equally spaced in the region $0 < -t/\text{GeV}^2 < 1$. Although we haven't played with the number of points in the sum rules (nor with their error), this choice led to a good balance between the FESR and the observables. The FESR represent a third of the total data point in the fit, 132 points, and contributes to a little bit more than a third of the chi-squared per degree of freedom, $\chi^2/d.o.f.|_{\text{FESR}} = 1.26$. There are 258 experimental data points, providing $\chi^2/d.o.f.|_{\text{exp.}} = 2.10$.

We hope that our solution presented in Tables III and IV will be a good starting point for a global fit of the experimental data in the whole energy range (from the resonance region to the Regge region) together with the analyticity constraints. Of course, once the low energy part of the model is varying, the LHS of the sum rules is no longer fixed. But once a cut-off $E_{\text{lab}}^{\text{max}}$, moments k and t values have been chosen, it should be straightforward to penalize, in the fit, the difference between the two side of the sum rules. Another possibility would be to parametrize only the imaginary part of the amplitudes and to reconstruct the real part from the dispersion relation. This procedure is however more involved as it imposes to reconstruct the real part before building the observables. One thus needs to perform the integral in each t values of the experimental data points. The first method requires to perform the integral only at predefined t values and is certainly more suitable for large database.

VIII. CONCLUSION

In this paper we analyzed the structure of the pion photoproduction amplitudes using the Finite Energy Sum Rules (FESR). In Sec. IV we compared the LHS of the FESR obtained from various models used in baryon analysis. Although some differences exist between the different models, we found that they all lead to the same qualitative results. The LHS of the FESR for all 12 isospin amplitudes present at most one extremum and at most one zero for $|t| < 1 \text{ GeV}^2$. We discussed the possible interpretation of this zero in Regge theory. We also found that in all models, isoscalar amplitudes violate the factorization of Regge poles.

In Sec. V we tested the hypothesis of a single Regge pole in each amplitude. The almost moment independence of the effective residue indicated that indeed the RHS of the FESR could be approximated by a single

Regge pole at leading approximation. We used these residues extracted from the FESR to predict the observables at high energy. We saw that the t -dependence of the differential cross section is well predicted by the low-energy models. The prediction for the asymmetry, sensitive to unnatural exchanges and next-to-leading Regge contributions, however is less reliable. There is then room for improvement in the unnatural amplitudes. With this perspective, the sum rules and the high-energy data could certainly improve the baryon analysis.

Finally in Sec. VII we built a flexible model allowing us to fit the FESR and the high-energy observables. Our solution involves the minimum Regge content in each amplitude: a leading Regge pole, whose trajectory is constrained around the expected values and, in the natural exchange amplitude, a additional cut/daughter-like term. The latter allowed us to match the zero pattern in the LHS of the FESR and to describe the high-energy observables.

When extracting the properties of baryon resonances in the 2-3 GeV region, the number of relevant partial waves grows and, with them, the number of parameters in the model. The technique we developed in this paper will certainly help to constrain this growing number of parameters. The solution we presented would be a good starting point to perform a joint fit of the low and high-energy data *via* the FESR, and eventually lead to a better understanding of the excited baryon spectrum. To this purpose, we made available our solution online on the JPAC website [63]. The user also has the possibility to upload his multipoles and display the resulting FESR.

Beyond baryon spectroscopy, the constraints provided by analyticity will be essential in the search of exotic mesons. We are therefore currently extending the method presented in this paper to beam fragmentation reactions [64].

ACKNOWLEDGMENTS

We acknowledge discussions with M. Döring, L. Tiator, A. Sarantsev, T. Sato and R. Workman about the low-energy models used in this study. This material is based upon work supported in part by the U.S. Department of Energy, Office of Science, Office of Nuclear Physics under contract DE-AC05-06OR23177. This work was also supported in part by the U.S. Department of Energy under Grant DE-FG0287ER40365, National Science Foundation under Grants PHY-1415459 and PHY-1205019, the IU Collaborative Research Grant and the Research Foundation Flanders (FWO-Flanders). CF-R work is supported in part by PAPIIT-DGAPA (UNAM) grant No. IA101717, by CONACYT (Mexico) grant No. 251817, and by Red Temática CONACYT de Física en Altas Energías (Red FAE, Mexico).

-
- [1] H. Al Ghouli *et al.* (GlueX), Phys. Rev. **C95**, 042201 (2017), arXiv:1701.08123 [nucl-ex].
- [2] M. Battaglieri *et al.* (CLAS), “Jlab approved experiment e12-11-005,” (2011), https://www.jlab.org/exp_prog/proposals/11/PR12-11-005.pdf.
- [3] L. Tiator, D. Drechsel, S. S. Kamalov, and M. Vanderhaeghen, Eur. Phys. J. ST **198**, 141 (2011), arXiv:1109.6745 [nucl-th].
- [4] W. J. Briscoe, A. E. Kudryavtsev, P. Pedroni, I. I. Strakovsky, V. E. Tarasov, and R. L. Workman, Phys. Rev. **C86**, 065207 (2012), arXiv:1209.0024 [nucl-th].
- [5] A. V. Anisovich, R. Beck, E. Klempt, V. A. Nikonov, A. V. Sarantsev, and U. Thoma, Eur. Phys. J. **A48**, 15 (2012), arXiv:1112.4937 [hep-ph].
- [6] D. Rönchen, M. Döring, F. Huang, H. Habertzettl, J. Haidenbauer, C. Hanhart, S. Krewald, U. G. Meißner, and K. Nakayama, Eur. Phys. J. **A50**, 101 (2014), [Erratum: Eur. Phys. J. **A51**, no.5, 63 (2015)], arXiv:1401.0634 [nucl-th].
- [7] H. Kamano, S. X. Nakamura, T. S. H. Lee, and T. Sato, Phys. Rev. **C88**, 035209 (2013), arXiv:1305.4351 [nucl-th].
- [8] A. V. Anisovich *et al.*, Eur. Phys. J. **A52**, 284 (2016), arXiv:1604.05704 [nucl-th].
- [9] A. C. Irving and R. P. Worden, Phys. Rept. **34**, 117 (1977).
- [10] R. Dolen, D. Horn, and C. Schmid, Phys. Rev. **166**, 1768 (1968).
- [11] R. Dolen, D. Horn, and C. Schmid, Phys. Rev. Lett. **19**, 402 (1967).
- [12] J. P. Ader, M. Capdeville, and P. Salin, Nucl. Phys. **B3**, 407 (1967).
- [13] G. R. Goldstein and J. F. Owens, Phys. Rev. **D7**, 865 (1973).
- [14] G. R. Goldstein, J. F. Owens, and J. P. Rutherford, Nucl. Phys. **B57**, 18 (1973).
- [15] G. R. Goldstein and J. F. Owens, Nucl. Phys. **B71**, 461 (1974).
- [16] M. Guidal, J. M. Laget, and M. Vanderhaeghen, Nucl. Phys. **A627**, 645 (1997).
- [17] A. Sibirtsev, J. Haidenbauer, S. Krewald, T. S. H. Lee, U.-G. Meißner, and A. W. Thomas, Eur. Phys. J. **A34**, 49 (2007), arXiv:0706.0183 [nucl-th].
- [18] A. Sibirtsev, J. Haidenbauer, S. Krewald, U. G. Meißner, and A. W. Thomas, Eur. Phys. J. **A41**, 71 (2009), arXiv:0902.1819 [hep-ph].
- [19] B. G. Yu, T. K. Choi, and W. Kim, Phys. Rev. **C83**, 025208 (2011), arXiv:1103.1203 [nucl-th].
- [20] V. Mathieu, G. Fox, and A. P. Szczepaniak, Phys. Rev. **D92**, 074013 (2015), arXiv:1505.02321 [hep-ph].
- [21] E. N. Argyres, A. P. Contogouris, J. P. Holden, and M. Svec, Phys. Rev. **D8**, 2068 (1973).
- [22] I. S. Barker, A. Donnachie, and J. K. Storrow, Nucl. Phys. **B79**, 431 (1974).
- [23] I. S. Barker and J. K. Storrow, Nucl. Phys. **B137**, 413 (1978).
- [24] J. D. Jackson and C. Quigg, Phys. Lett. **29B**, 236 (1969).
- [25] M. Hontebeyrie, J. Procureur, and P. Salin, Nucl. Phys. **B55**, 83 (1973).
- [26] M. Rahnama and J. K. Storrow, J. Phys. **G17**, 243 (1991).
- [27] R. Worden, Nucl. Phys. **B37**, 253 (1972).
- [28] R. C. E. Devenish, D. H. Lyth, and W. A. Rankin, Phys. Lett. **52B**, 227 (1974).
- [29] I. M. Barbour and R. G. Moorhouse, Nucl. Phys. **B69**, 637 (1974).
- [30] I. M. Barbour and R. L. Crawford, Nucl. Phys. **B111**, 358 (1976).
- [31] I. M. Barbour, R. L. Crawford, and N. H. Parsons, Nucl. Phys. **B141**, 253 (1978).
- [32] R. Odorico, Nucl. Phys. **B101**, 480 (1975).
- [33] C. Patrignani *et al.* (Particle Data Group), Chin. Phys. **C40**, 100001 (2016).
- [34] J. Nys, V. Mathieu, C. Fernández-Ramírez, A. N. Hiller Blin, A. Jackura, M. Mikhasenko, A. Pilloni, A. P. Szczepaniak, G. Fox, and J. Ryckebusch (JPAC), Phys. Rev. **D95**, 034014 (2017), arXiv:1611.04658 [hep-ph].
- [35] V. Mathieu, I. V. Danilkin, C. Fernández-Ramírez, M. R. Pennington, D. Schott, A. P. Szczepaniak, and G. Fox, Phys. Rev. **D92**, 074004 (2015), arXiv:1506.01764 [hep-ph].
- [36] G. F. Chew, M. L. Goldberger, F. E. Low, and Y. Nambu, Phys. Rev. **106**, 1345 (1957).
- [37] P. D. B. Collins, *An Introduction to Regge Theory and High-Energy Physics*, Cambridge Monographs on Mathematical Physics (Cambridge Univ. Press, Cambridge, UK, 2009).
- [38] G. Cohen-Tannoudji, P. Salin, and A. Morel, Nuovo Cim. **A55**, 412 (1968).
- [39] J. S. Ball, Phys. Rev. **124**, 2014 (1961).
- [40] F. A. Berends, A. Donnachie, and D. L. Weaver, Nucl. Phys. **B4**, 1 (1967).
- [41] B. Pasquini, D. Drechsel, and L. Tiator, Eur. Phys. J. **A27**, 231 (2006), arXiv:nucl-th/0603006 [nucl-th].
- [42] R. G. Kennett, A. V. Barnes, G. C. Fox, R. L. Walker, O. I. Dahl, R. W. Kenney, A. Ogawa, and M. Pripstein, Nucl. Phys. **B284**, 653 (1987).
- [43] A. V. Barnes, G. C. Fox, R. G. Kennett, R. L. Walker, O. I. Dahl, R. A. Johnson, R. W. Kenney, A. Ogawa, and M. Pripstein, Phys. Rev. Lett. **41**, 1260 (1978).
- [44] P. Noelle, Prog. Theor. Phys. **60**, 778 (1978).
- [45] C. collaboration (CLAS), “in preparation,” (2017).
- [46] J. Mandula, J. Weyers, and G. Zweig, Ann. Rev. Nucl. Part. Sci. **20**, 289 (1970).
- [47] S. Godfrey and N. Isgur, Phys. Rev. **D32**, 189 (1985).
- [48] R. L. Anderson, D. Gustavson, J. R. Johnson, I. Overman, D. Ritson, B. H. Wiik, and D. Worcester, Phys. Rev. **D4**, 1937 (1971).
- [49] B. Barish, R. Gomez, D. Kreinick, C. Peck, J. Pine, F. Sciulli, B. Sherwood, A. Tollestrup, and K. Young, Phys. Rev. **D9**, 566 (1974).
- [50] G. C. Bolon, C. Garelick, S. Homma, R. Lewis, W. Lobar, D. Luckey, L. S. Osborne, R. Schwitters, and J. Uglum, Phys. Rev. Lett. **18**, 926 (1967).
- [51] W. Braunschweig, H. Dinter, W. Erlewein, H. Frese, K. Luebelsmeyer, H. Meyer-Wachsmuth, C. C. Morehouse, D. Schmitz, A. Schultz Von Dratzig, and G. Wesels, Nucl. Phys. **B51**, 157 (1973).
- [52] A. M. Osborne, A. Brownam, K. Hanson, W. T. Meyer, A. Silverman, F. E. Taylor, and N. Horwitz, Phys. Rev.

- Lett. **29**, 1621 (1972).
- [53] G. C. Bolon, D. Bellenger, W. Lobar, D. Luckey, L. S. Osborne, and R. Schwitters, Phys. Rev. Lett. **27**, 964 (1971).
- [54] R. L. Anderson, D. Gustavson, J. R. Johnson, I. Overman, D. Ritson, B. H. Wiik, R. Talman, J. K. Walker, and D. Worcester, Phys. Rev. Lett. **25**, 1218 (1970).
- [55] P. S. L. Booth, G. R. Court, B. Craven, R. Gamet, P. J. Hayman, J. R. Holt, A. P. Hufton, J. N. Jackson, J. H. Norem, and W. H. Range, Phys. Lett. **38B**, 339 (1972).
- [56] M. Deutsch, L. Golub, P. Kijewski, D. Potter, D. J. Quinn, and J. Rutherford, Phys. Rev. Lett. **29**, 1752 (1972).
- [57] A. Boyarski, F. Bulos, W. Busza, R. E. Diebold, S. D. Ecklund, G. E. Fischer, J. R. Rees, and B. Richter, Phys. Rev. Lett. **20**, 300 (1968).
- [58] J. P. Dowd, D. O. Caldwell, K. Heinloth, and T. R. Sherwood, Phys. Rev. Lett. **18**, 414 (1967).
- [59] P. Heide, *Photoeinfacherzeugung geladener π -Mesonen bei kleinen Impulsüberträgen im Energiebereich zwischen 2.6 und 6.0 GeV*, Ph.D. thesis, Hamburg U. (1969).
- [60] D. Sherden, R. Siemann, C. K. Sinclair, D. J. Quinn, J. P. Rutherford, and M. A. Shupe, Phys. Rev. Lett. **30**, 1230 (1973).
- [61] Z. Bar-Yam, J. de Pagter, M. M. Hoenig, W. Kern, D. Luckey, and L. S. Osborne, Phys. Rev. Lett. **19**, 40 (1967).
- [62] C. Geweniger, P. Heide, U. Kötz, R. A. Lewis, P. Schmueser, H. J. Skronn, H. Wahl, and K. Wegener, Phys. Lett. **B29**, 41 (1969).
- [63] V. Mathieu, *Proceedings, 16th International Conference on Hadron Spectroscopy (Hadron 2015): Newport News, Virginia, USA, September 13-18, 2015*, AIP Conf. Proc. **1735**, 070004 (2016), arXiv:1601.01751 [hep-ph].
- [64] V. P. *et al.* (JPAC), “in preparation,” (2017).